

Tracking the risk of a deployed model and detecting harmful distribution shifts

Aleksandr Podkopaev^{1,2}, Aaditya Ramdas^{1,2}
 Department of Statistics & Data Science¹
 Machine Learning Department²
 Carnegie Mellon University
 {podkopaev, aramdas}@cmu.edu

October 13, 2021

Abstract

When deployed in the real world, machine learning models inevitably encounter changes in the data distribution, and certain—but not all—distribution shifts could result in significant performance degradation. In practice, it may make sense to ignore benign shifts, under which the performance of a deployed model does not degrade substantially, making interventions by a human expert (or model retraining) unnecessary. While several works have developed tests for distribution shifts, these typically either use non-sequential methods, or detect arbitrary shifts (benign or harmful), or both. We argue that a sensible method for firing off a warning has to both (a) detect harmful shifts while ignoring benign ones, and (b) allow continuous monitoring of model performance without increasing the false alarm rate. In this work, we design simple sequential tools for testing if the difference between source (training) and target (test) distributions leads to a significant drop in a risk function of interest, like accuracy or calibration. Recent advances in constructing time-uniform confidence sequences allow efficient aggregation of statistical evidence accumulated during the tracking process. The designed framework is applicable in settings where (some) true labels are revealed after the prediction is performed, or when batches of labels become available in a delayed fashion. We demonstrate the efficacy of the proposed framework through an extensive empirical study on a collection of simulated and real datasets.

Contents

1	Introduction	2
2	Sequential testing for a significant risk increase	3
2.1	Casting the detection of risk increase as a sequential hypothesis test	4
2.2	Sequential testing via sequential estimation	5
3	Experiments	6
3.1	Simulated data	6
3.2	Real data	8
4	Discussion	10
A	Brier score in the multiclass setting	13
B	Proofs	16
C	Primer on the upper and lower confidence bounds	16

D Experiments on simulated data	18
D.1 Brier score as a target metric	19
E Experiments on real datasets	20
E.1 MNIST-C simulation	20
E.2 CIFAR-10-C simulation	20

1 Introduction

Developing a machine learning system usually involves data splitting where one of the labeled folds is used to assess its generalization properties. Under the assumption that the incoming test instances (target) are sampled independently from the same underlying distribution as the training data (source), estimators of various performance metrics, such as accuracy, reliably reflect the truth. However, a model deployed in the real world inevitably encounters variability in the input distribution, a phenomenon referred to as *dataset shift*; see the book by [15]. Special cases include covariate shift [18] and label shift [17]. While testing whether a distribution shift is present has been studied both in offline [4, 9, 16] and online [20–22] settings, a natural question is whether an intervention is required once there is evidence that a shift has occurred.

Sometimes, structured shifts can be handled in a post-hoc fashion without performing expensive actions, such as model retraining. One example arises within the context of distribution-free uncertainty quantification where the goal is to supplement predictions of a model with a measure of uncertainty valid under minimal assumptions. Recent works [6, 14, 19] describe ways of correcting for covariate and label shifts that do not require labeled data from the target. However, both aforementioned shifts impose restrictive assumptions on the possible changes in the underlying probability distribution, insisting either that $P(Y|X)$ stays unchanged (covariate shift) or $P(X|Y)$ stays unchanged (label shift), allowing the change only in either $P(X)$ or $P(Y)$. While distribution shifts constantly occur in practice, they generally have a more complex nature. In medical diagnosis, $P(Y)$ and $P(X|Y = y)$ could describe the prevalence of certain diseases in the population and the corresponding symptoms. One might reasonably expect not only the former to change over time (due to potential epidemiological states) but also the latter (due to potential mutations), violating the covariate/label shift assumptions.

A related question is whether labeled data from one distribution can be used for training a model in a way that it generalizes well to another distribution where it is hard to obtain labeled examples. Importance-weighted risk minimization can yield models with good generalization properties on the target domain, but the corresponding guarantees typically become vacuous under many real-world scenarios. Adversarial training schemes [3, 26] for deep learning models often yield models with reasonable performance on the target.

A trustworthy machine learning system has to be supplemented with a set of tools designed to raise alarms whenever critical changes take place. Vovk et al. [23] argue that a predictive model has to be retrained once the i.i.d. assumption becomes violated and design the corresponding online testing protocols. However, naive testing whether a distribution shift is present is not fully practical since it does not take into account the malignancy of a shift [16]. A user is typically interested in how a model performs according to some metrics. In a *benign* scenario, the one where those are not significantly affected by a shift, costly actions, e.g., retraining, become unnecessary. A model capable of separating classes sufficiently well on the source distribution can often generalize well to the target, which we illustrate for covariate and label shifts on Figures 1a and 1b respectively.

In this work, we argue for triggering a warning once the non-regularities in the data generating distribution lead to a statistically significant increase in the risk function of interest. We design theoretically tractable tools for nonparametric sequential testing for an unfavorable change in a chosen risk function of any black-box model which allows rigorous reasoning whether a human expert has to intervene in a data-adaptive way. The proposed testing protocols are based on the time-uniform confidence sequences [8, 25] that efficiently aggregate statistical evidence collected over the monitoring process. The procedure can be deployed in settings where (some) true labels are revealed after the prediction is performed, or where the sets of the true labels are observed in a delayed fashion. During the preparation of our paper, we also noticed a very recent preprint [10] on broadly the same topic. While they also advise against testing naively for the presence of a

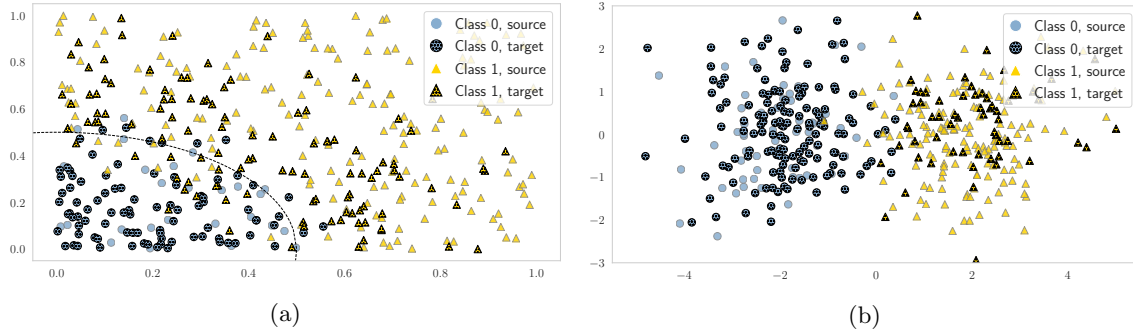


Figure 1: Samples from the source and the target (hatched) distributions under benign (a) covariate and (b) label shifts. (a) $X \sim \text{Unif}([0, 1] \times [0, 1])$ on the source and $X_i \sim \text{Beta}(1, 2)$, $i = 1, 2$ on the target. Labels satisfy: $\mathbb{P}(Y = 1 \mid X = x) = \mathbb{P}(x_1^2 + x_2^2 + \varepsilon \geq 1/4)$ where $\varepsilon \sim \mathcal{N}(0, 0.01)$. (b) Marginal probability of class 1 changes from $\pi_1^S = 0.7$ on the source to $\pi_1^T = 0.3$ on the target. Covariates satisfy: $X \mid Y = y \sim \mathcal{N}(\mu_y, I_2)$, where $\mu_0 = (-2, 0)^\top$, $\mu_1 = (2, 0)^\top$. In both cases, a model capable of separating well data from the source will generalize well to the target.

shift, their approach is different from ours as it (a) is based on measuring the malignancy of a shift based on outlier scores, and (b) is non-sequential.

The structure of the paper is the following. In Section 2, we set up appropriate notations and discuss various loss functions of practical interest. We also study several generalizations of the Brier score [2] to multiclass classification. We formalize the task as a sequential hypothesis test (Section 2.1) and describe our solution based on sequential estimation (Section 2.2). In Section 3, we evaluate the proposed framework on both simulated (Section 3.1) and real data (Section 3.2).

2 Sequential testing for a significant risk increase

Let \mathcal{X} and $\mathcal{Y} = \{1, \dots, K\}$ denote the covariate and label spaces respectively. Consider predictors $f : \mathcal{X} \rightarrow \Delta^{|\mathcal{Y}|-1}$ which output a distribution $f(x)$ over labels on any given input $x \in \mathcal{X}$. Let $\hat{y}(x; f) := \arg \max_{k \in \mathcal{Y}} f_k(x)$ denote the label prediction of a model f on a given input $x \in \mathcal{X}$. Let $\ell(\cdot, \cdot)$ be a bounded loss function chosen to be monitored, with $R(f) := \mathbb{E}[\ell(f(X), Y)]$ denoting the corresponding expected loss, or the risk of a predictor f . Despite the focus on classification, the methods in this paper do extend straightforwardly to other problems with bounded observations or bounded loss functions. We use the following bounded classification losses in our simulations.

Multiclass losses The most common example is arguably the misclassification loss and its generalization that allows for a label-dependent cost of a mistake:

$$\ell^{\text{mis}}(f(x), y) := \mathbb{1}\{\hat{y}(x; f) \neq y\} \in \{0, 1\}, \quad \ell^{\text{w-mis}}(f(x), y) := \ell_y \cdot \mathbb{1}\{\hat{y}(x; f) \neq y\} \in [0, L],$$

where $\{\ell_k\}_{k \in \mathcal{Y}}$ is a collection of per-class costs and $L = \max_{k \in \mathcal{Y}} \ell_k$. The loss function $\ell^{\text{w-mis}}$ is more relevant to high-stakes decision settings and imbalanced classification.

However, high accuracy alone can often be insufficient. The Brier score (squared error), introduced initially for the binary setting [2], is commonly employed to encourage calibration of probabilistic classifiers. For multiclass problems, one could consider the mean-squared error of the whole output vector:

$$\ell^{\text{brier}}(f(x), y) := \frac{1}{2} \|f(x) - h(y)\|^2 \in [0, 1], \quad (1)$$

where $h : \mathcal{Y} \rightarrow \{0, 1\}^{|\mathcal{Y}|}$ is a one-hot label encoder: $h_{y'}(y) = \mathbb{1}\{y' = y\}$ for $y, y' \in \mathcal{Y}$. Top-label calibration [5] restricts attention to the entry corresponding to the top-ranked label. A closely related loss function, which we call the *top-label Brier score*, is the following:

$$\ell^{\text{brier-top}}(f(x), y) := (f_{\hat{y}(x; f)}(x) - \mathbb{1}\{\hat{y}(x; f) = y\})^2 = (f_{\hat{y}(x; f)}(x) - h_{\hat{y}(x; f)}(y))^2 \in [0, 1]. \quad (2)$$

Alternatively, instead of the top-ranked label, one could focus only on the entry corresponding to the true class. It gives rise to another loss function which we call the *true-class* Brier score:

$$\ell^{\text{brier-true}}(f(x), y) := (f_y(x) - 1)^2 \in [0, 1]. \quad (3)$$

The loss functions ℓ^{brier} , $\ell^{\text{brier-top}}$, $\ell^{\text{brier-true}}$ trivially reduce to the same loss function in the binary setting. We refer the reader to Appendix A for derivations and some illustrative examples.

Set-valued predictors The set of tools we propose can also be used on top of set-valued predictors that output a subset of \mathcal{Y} as a prediction. Those naturally arise in multilabel classification, where more than a single label can be the correct one, or as a result of post-processing point predictors, which could target covering the correct label of a test point with high probability [22] or controlling other notions of risk [1] like the miscoverage loss:

$$\ell^{\text{miscov}}(y, S(x)) = \mathbb{1}\{y \notin S(x)\}, \quad (4)$$

where $S(x)$ denotes the output of a set-valued predictor on any given input $x \in \mathcal{X}$. When considering multilabel classification, relevant loss functions include the symmetric difference between the output and the set of true labels, false negative rate and false discovery rate.

2.1 Casting the detection of risk increase as a sequential hypothesis test

We design a set of tools that trigger a warning whenever the risk on the target domain exceeds the risk on the source by a non-negligible amount specified in advance. For example, alerting a user could happen once it is possible to conclude with certain confidence that the misclassification error on the target has increased by 10% when compared against the source. Shifts that lead to a decrease or an insignificant increase in the risk are then treated as benign. Formally, it corresponds to designing a sequential test for the following pair of hypotheses:

$$H_0 : R_T(f) \leq R_S(f) + \varepsilon_{\text{tol}} \quad \text{vs.} \quad H_1 : R_T(f) > R_S(f) + \varepsilon_{\text{tol}}, \quad (5)$$

where $\varepsilon_{\text{tol}} \geq 0$ is an acceptable tolerance level, and $R_S(f)$ and $R_T(f)$ stand for the risk of f on the source and target domains respectively. A sequential test takes the data as input and outputs a sequence of 0s (continue) and 1s (reject the null and stop) such that if the null H_0 is true, the probability that it ever outputs a 1 and stops (false alarm) is at most δ , meaning that it never outputs a 1 with high probability, and thus runs forever. Formally, a level- δ sequential test Φ defined as a mapping $\bigcup_{n=1}^{\infty} \mathcal{Z}^n \rightarrow \{0, 1\}$ must satisfy: $\mathbb{P}_{H_0}(\exists t \geq 1 : \Phi(Z_1, \dots, Z_t) = 1) \leq \delta$. Note that the sequential nature of a test is critical here as we aim to develop a framework capable of continuously updating inference as data from the target is collected, making it suitable for many practical scenarios. We distinguish between two important settings when we assume that the target data either satisfies (a) an i.i.d. assumption (under the same or different distribution as the source) or (b) only an independence assumption. While the i.i.d. assumption may be arguably reasonable on the source, it is usually less realistic on the target, since in practice, one may expect the distribution to drift slowly in a non-i.i.d. fashion instead of shifting sharply but staying i.i.d. Under setting (b), the quantity of interest on the target is the *running risk*:

$$R^{(t)}(f) = \frac{1}{t} \sum_{i=1}^t \mathbb{E}[\ell(f(X'_i), Y'_i)], \quad t \geq 1,$$

and the goal transforms into designing a more general test for the following pair of hypotheses:

$$H_0 : R_T^{(t)}(f) \leq R_S(f) + \varepsilon_{\text{tol}}, \quad \forall t \geq 1, \quad \text{vs.} \quad H_1 : \exists t^* \geq 1 : R_T^{(t^*)}(f) > R_S(f) + \varepsilon_{\text{tol}}. \quad (6)$$

When considering other notions of risk beyond the misclassification error, one could also be interested in relative changes in the risk, and thus a sequential test for the following pair of hypotheses:

$$H'_0 : R_T(f) \leq (1 + \varepsilon_{\text{tol}})R_S(f), \quad \text{vs.} \quad H'_1 : R_T(f) > (1 + \varepsilon_{\text{tol}})R_S(f). \quad (7)$$

The proposed framework handles all of the aforementioned settings as we discuss next. The most classical approach for sequential testing is the sequential probability ratio test (SPRT) due to Wald [24]. However, this

can only be applied, even for a point null and a point alternative, when the relevant underlying distributions are known. While extensions of the SPRT exist to the composite null and alternative (our setting above), these also require knowledge of the distributions of the test statistics (e.g., empirical risk) under the null and alternative, and being able to maximize the likelihood. Clearly, we make no distributional assumptions and so we require a more nonparametric approach. We perform sequential testing via the dual problem of nonparametric sequential estimation, a problem for which there has been much recent progress to draw from.

2.2 Sequential testing via sequential estimation

When addressing a particular prediction problem, the true risk on neither the source nor the target domains is known. Performance of a model on the source domain is usually assessed through a labeled held-out sample of a fixed size n_S : $\{(X_i, Y_i)\}_{i=1}^{n_S}$. For a chosen loss ℓ and a learnt predictor f , we use $Z := \ell(f(X), Y)$ to denote the losses on individual data points. We can write:

$$R_S(f) + \varepsilon_{\text{tol}} = \widehat{R}_S(f) + \left(R_S(f) - \widehat{R}_S(f)\right) + \varepsilon_{\text{tol}},$$

where $\widehat{R}_S(f) := (\sum_{i=1}^{n_S} Z_i) / n_S$. For any fixed tolerance level $\delta_S \in (0, 1)$, classic concentration results can be used to obtain an upper confidence bound $\varepsilon_{\text{appr}}$ on the difference $R_S(f) - \widehat{R}_S(f)$, and thus to conclude that with probability at least $1 - \delta_S$:

$$R_S(f) + \varepsilon_{\text{tol}} \leq \widehat{U}_S(f) + \varepsilon_{\text{tol}}, \quad (8)$$

where $\widehat{U}_S(f) = \widehat{R}_S(f) + \varepsilon_{\text{appr}}$. In the worst-case, $\Omega(1/\varepsilon_{\text{appr}}^2)$ points from the source are needed to guarantee $\varepsilon_{\text{appr}}$ -approximation due to Hoeffding's inequality, but such guarantee can still be quite loose in a number of settings. If accuracy is a guiding performance metric, one would rarely deploy models performing only slightly better than prediction by chance. The individual losses might satisfy the low-variance property that can subsequently be exploited by variance-adaptive confidence bounds [8, 25]. Tighter bounds increase the power of the testing procedure, or in words, allows to trigger a warning much earlier if needed.

In contrast, the estimator of the risk on the target has to be updated online as losses on test instances $(X'_1, Y'_1), (X'_2, Y'_2), \dots$ are observed. The sequential nature of this monitoring process invalidates the classic concentration results as the size of a sample to be used for estimation can not be specified in advance. Time-uniform confidence sequences retain validity under adaptive data collection settings. For any chosen $\delta_T \in (0, 1)$, those yield a time-uniform lower confidence bound on $R_T(f)$:

$$\mathbb{P}\left(\exists t \geq 1 : R_T(f) < \widehat{L}_T^{(t)}(f)\right) \leq \delta_T,$$

where $\widehat{L}_T^{(t)}(f)$ is the bound constructed after processing t test points. We typically set $\delta_S = \delta_T = \delta/2$, where δ refers to the desired type I error. Under the independence assumption (equation 6), we invoke time-uniform variance-adaptive lower bound on the running risk $R_T^{(t)}(f)$ due to Howard et al. [8]. The testing protocol is summarized in Algorithm 1, and a brief review of the key concentration results used in this work can be found in Appendix C.

Algorithm 1 Sequential testing for an absolute increase in the risk

Input: Predictor f , loss ℓ , tolerance level ε_{tol} , sample from the source $\{(X_i, Y_i)\}_{i=1}^{n_S}$

1: **procedure**

2: Compute the upper confidence bound on the source risk $\widehat{U}_S(f)$;

3: **for** $t = 1, 2, \dots$ **do**

4: Compute the lower confidence bound on the target risk $\widehat{L}_T^{(t)}(f)$;

5: **if** $\widehat{L}_T^{(t)}(f) > \widehat{U}_S(f) + \varepsilon_{\text{tol}}$ **then**

6: Reject H_0 (equation 5) and fire off a warning.

Testing for a relative increase in the risk is performed by replacing the line 5 in the Algorithm 1 by the condition $\widehat{L}_T^{(t)}(f) > (1 + \varepsilon_{\text{tol}})\widehat{U}_S(f)$. For both cases, the proposed test controls type I error as formally stated next. The proof is presented in Appendix B.

Proposition 1. Fix any $\delta \in (0, 1)$. Let $\delta_S, \delta_T \in (0, 1)$ be chosen in a way such that $\delta_S + \delta_T = \delta$. Let $\widehat{L}_T^{(t)}(f)$ define a time-uniform lower confidence bound on $R_T^{(t)}(f)$ at level δ_T after processing t data points ($t \geq 1$), and let $\widehat{U}_S(f)$ define an upper confidence bound on $R_S(f)$ at level δ_S . Then:

$$\begin{cases} \mathbb{P}_{H_0} \left(\exists t \geq 1 : \widehat{L}_T^{(t)}(f) > \widehat{U}_S(f) + \varepsilon_{tol} \right) \leq \delta, \\ \mathbb{P}_{H'_0} \left(\exists t \geq 1 : \widehat{L}_T^{(t)}(f) > (1 + \varepsilon_{tol})\widehat{U}_S(f) \right) \leq \delta, \end{cases} \quad (9)$$

that is, the procedure described in Algorithm 1 controls the type I error for testing the hypotheses H_0 (equation 5 and equation 6) and H'_0 (equation 7).

Remark 1. Both the testing protocol (Algorithm 1) and the corresponding guarantee (Proposition 1) are stated in a form which requires the lower bound on the target risk to be recomputed after processing each test point. More generally, test data could be processed in minibatches of size $m \geq 1$. Similarly, the initial sample size could be replaced with some other initial size $t_0 \geq 1$.

Remark 2. The above type I error guarantee (equation 9) holds under continuous monitoring. This goes beyond standard guarantees for a fixed-time test, for which type I error control only holds when the sample size is fixed in advance, and not under continuous monitoring. We can define a stopping time of a sequential test in Algorithm 1 as:

$$N(\delta) := \inf \left\{ t \geq 1 : \widehat{L}_T^{(t)}(f) > \widehat{U}_S(f) + \varepsilon_{tol} \right\},$$

and restate the guarantee in equation 9 as: $\mathbb{P}_{H_0} (N(\delta) < \infty) \leq \delta$, that is the probability of ever raising a false alarm is at most δ .

From sequential testing to changepoint detection Results due to Lorden [12] allow to transform a valid sequential test into a changepoint detection procedure with certain guarantees. The key characteristics of changepoint detection procedures are *average run length* (ARL), or average time to a false alarm, and *average detection delay* (ADD). One way to convert a sequential test into a detection procedure is by running a separate test starting at each time point $t = 1, 2, \dots$, and claiming a change whenever the first one of the tests rejects the null. Subsequently, these tests yield a sequence of stopping variables $N_1(\delta), N_2(\delta), \dots$. The corresponding stopping time is defined as:

$$N^*(\delta) := \inf_{k=1,2,\dots} (N_k(\delta) + (k - 1)).$$

Lorden [12] established a lower bound on the (worst-case) ARL of such changepoint detection procedure of the form: $\mathbb{E}_{H_0} [N^*(\delta)] \geq 1/\delta$. The (worst-case) average detection delay is defined as:

$$\overline{\mathbb{E}}_1 N(\delta) = \sup_{m \geq 1} \text{ess sup} \mathbb{E}_m \left[(N(\delta) - (m - 1))_+ \mid (X'_1, Y'_1), \dots, (X'_{m-1}, Y'_{m-1}) \right],$$

where \mathbb{E}_m denotes expectation under P_m , the distribution of a sequence $(X'_1, Y'_1), (X'_1, Y'_1), \dots$ under which (X'_m, Y'_m) is the first term from a shifted distribution.

3 Experiments

In Section 3.1, we study the performance of the testing procedure on a collection of simulated datasets. First, we consider the setting where the i.i.d. assumption on the target is satisfied, and then relax it to the independence assumption. In Section 3.2, we evaluate the framework on real data.

3.1 Simulated data

Tracking the risk under the i.i.d. assumption Here we consider inducing label shift on the target domain and emulate a setting where it noticeably harms the accuracy of a predictor by modifying the setup

from Section 1 through updating the class centers to: $\mu_0 = (-1, 0)^\top$, $\mu_1 = (1, 0)^\top$, making the classes largely overlap. The Bayes-optimal predictor on the source domain is:

$$f^*(x) = \frac{\pi_1^S \cdot \varphi(x; \mu_1, I_2)}{\pi_0^S \cdot \varphi(x; \mu_0, I_2) + \pi_1^S \cdot \varphi(x; \mu_1, I_2)}, \quad (10)$$

where $\varphi(x; \mu_i, I_2)$ denotes the probability density function of a Gaussian random vector with mean μ_i , $i = 0, 1$ and an identity covariate matrix. The misclassification risk of f^* on the target is:

$$\begin{aligned} \mathbb{P}_T(f^*(X) \neq Y) &= \mathbb{P}\left(X^\top(\mu_1 - \mu_0) < \log\left(\frac{\pi_0^S}{\pi_1^S}\right) + \frac{1}{2}(\|\mu_1\|_2^2 - \|\mu_0\|_2^2) \mid Y = 1\right) \cdot \pi_1^T \\ &+ \mathbb{P}\left(X^\top(\mu_1 - \mu_0) \geq \log\left(\frac{\pi_0^S}{\pi_1^S}\right) + \frac{1}{2}(\|\mu_1\|_2^2 - \|\mu_0\|_2^2) \mid Y = 0\right) \cdot \pi_0^T. \end{aligned}$$

In words, the risk is a linear function of π_1^T , the marginal probability of class 1 on the target. For three different values of π_1^S , the marginal probability of class 1 on the source, we illustrate how label shift affects the misclassification risk of the Bayes-optimal predictor on Figure 2a. Notice that it does not necessarily increase the misclassification risk. To analyze the power of the testing framework, we proceed with $\pi_1^S = 0.25$ and the corresponding Bayes-optimal rule. On Figure 2b, we compare upper confidence bounds $\hat{U}_S(f)$ on the true risk on the source obtained by invoking different concentration results. The variance-adaptive upper confidence bounds adapt to the low-variance property and are much tighter than the non-adaptive Hoeffding’s bound.

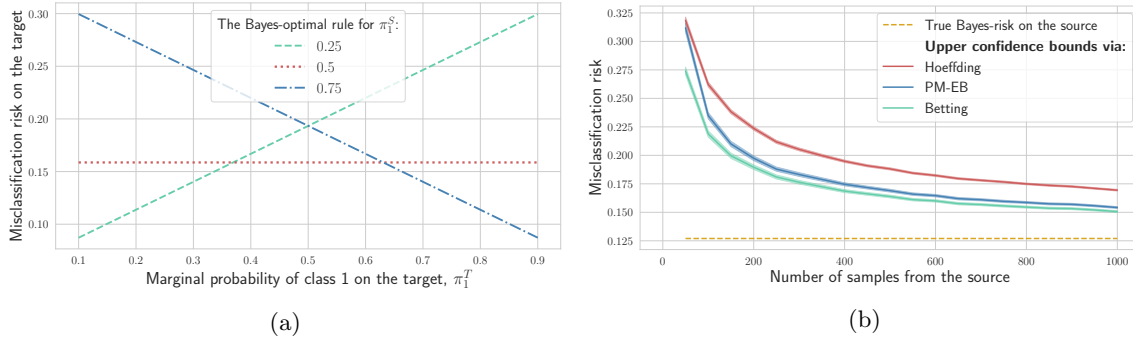


Figure 2: (a) The misclassification risk on the target of the Bayes-optimal predictors for three values of π_1^S . Notice that label shift does not necessarily lead to an increase in the risk. (b) Upper confidence bounds $\hat{U}_S(f)$ on the misclassification risk on the source obtained via several possible concentration results. For each sample size, the results are aggregated over 1000 random data draws. The variance-adaptive confidence bounds are much tighter when compared against the non-adaptive one.

Next, we fix $\varepsilon_{\text{tol}} = 0.05$, which corresponds to treating a 5% drop in accuracy as significant, and use $n_S = 1000$ data points from the source to compute the upper confidence bound on the source risk. For 20 values of π_1^T , evenly spaced in the interval $[0.1, 0.9]$, we sample data from the target distribution in batches of 50 points, with maximum number of points fixed to be 2000. On Figure 3a, we track the proportion of null rejections after repeating the process 250 times. On Figure 3b, we illustrate the average size of a sample from the target that was needed to reject the null. With a stronger label shift being more harmful to accuracy as a target metric, the results confirm that tighter bounds demonstrate better detection properties and generally require less samples to do so, and the most powerful test utilizes the bounds based on betting [25]. We refer the reader to Appendix D for a similar analysis performed for the Brier score as a target metric.

Tracking beyond the i.i.d. setting (distribution drift) Here we consider testing whether the running risk on the target exceeds the risk on the source (equation 6). First, we keep the data generation pipeline as before and fix $\pi_1^T = 0.75$, that is the data are still sampled in an i.i.d. fashion. We compare lower confidence bounds on the target risk studied before against the one due to conjugate-mixture empirical-Bernstein [8].

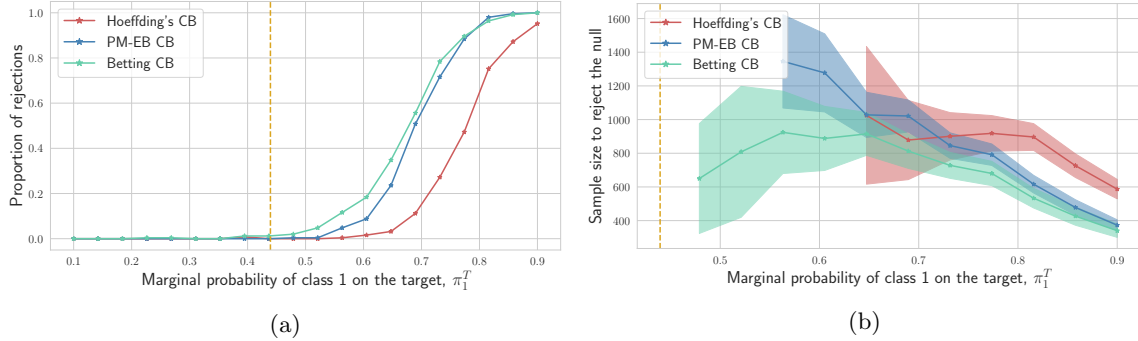


Figure 3: (a) Proportion of null rejections when testing for an increase in the misclassification risk after processing 2000 samples from a shifted distribution. The vertical dashed yellow line separates null vs alternative settings, and the alternatives correspond to $\pi_1^T \gtrsim 0.44$. Comparing procedures that rely on different confidence bounds (CB), we observe those based on variance-adaptive CBs have higher power. (b) Size of a sample from the target that was needed to reject the null. Invoking tighter concentration results allows to raise an alarm after processing less samples from the target.

While it yields a lower bound on the running mean of the random variables, the flexibility here comes at a higher computational cost. On Figure 4a, we illustrate that the lower confidence bounds based on betting are generally tighter. Similar results hold for the Brier score as a target metric (Appendix D.1).

Next, we relax the i.i.d. assumption on the target to the independence assumption, which invalidates computing the lower bound on the running risk on the target via betting, and thus we refer to the one based on conjugate-mixture empirical-Bernstein. We modify the data generation pipeline the following way: starting with $\pi_1^T = 0.25$, we increase π_1^T by 0.1 after sampling each 200 instances, until it reaches the value 0.85. Here, instead of changing sharply, the target distribution gradually drifts from the source. The results of running the framework for this setting are presented on Figure 4b.

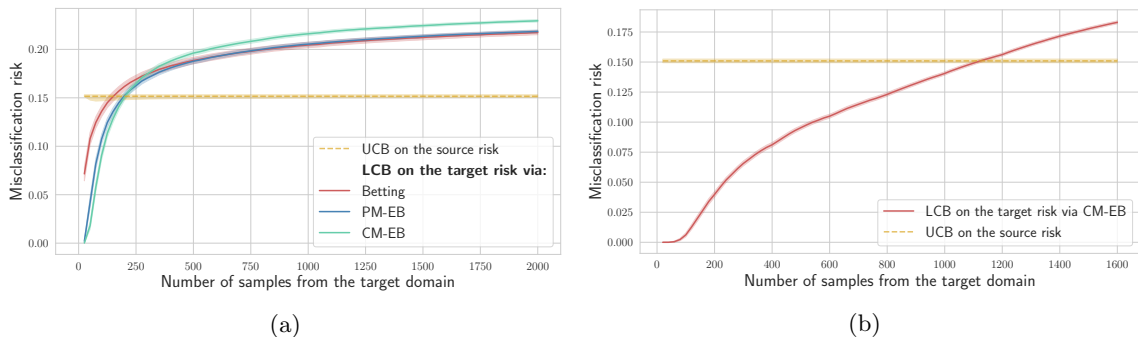


Figure 4: (a) Different lower confidence bounds on the target risk when the i.i.d. assumption is satisfied. The horizontal dashed red line indicated an upper confidence bound $\widehat{U}_S(f)$ on the misclassification risk on the source. (b) Running the testing framework when the target distribution gradually drifts, and thus only the independence assumption is satisfied. Procedure based on conjugate-mixture empirical-Bernstein consistently detects a harmful increase in the running risk.

3.2 Real data

Next, we evaluate the testing framework on real data. In deep learning, out-of-distribution robustness is often assessed based on a model performance gap between the original data (used for training) and data to which various perturbations have been applied. We focus on two image classification datasets with induced corruptions: MNIST-C [13] and CIFAR-10-C [7, 11]. We illustrate an example of a clean MNIST image

on Figure 5a along with its corrupted versions after applying *motion blur*, blur along a random direction (Figure 5b), *translate*, affine transformation along a random direction (Figure 5c), and *zigzag*, randomly oriented zigzag over an image (Figure 5d). For CIFAR-10-C, we consider corrupting original images by applying the *fog* effect with 3 levels of severity as illustrated on the bottom row of Figure 5. While corruptions are clearly visible to a human eye but are not expected to hurt classification performance significantly, it is different when such images passed to a predictive model. In both cases, we consider the settings when either clean test samples or ones with induced corruptions are passed as input to networks trained on clean datasets. For the simulations that follow, we refer to the betting-based upper confidence bounds on the risk for the source, and to the lower confidence bounds on the running risk that are due to conjugate-mixture empirical-Bernstein for the target.

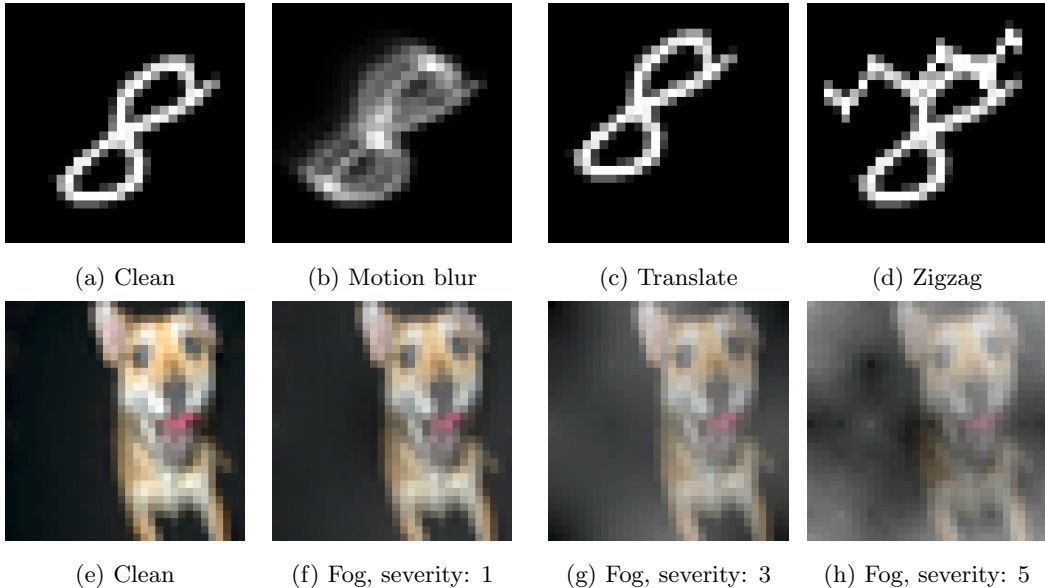


Figure 5: (a)-(d) example of a MNIST-C image; (e)-(h) example of a CIFAR-10-C image.

Tracking the risk of a point predictor on MNIST-C dataset We train a shallow CNN on clean MNIST data, and run the framework testing whether the misclassification risk increases by $\epsilon_{\text{tol}} = 0.1$, or 10%, passing data in batches of 50 points either from the original or shifted distribution to the network as input. We refer the reader to Appendix E for details regarding the network architecture and the training process. On Figure 6a, we illustrate the results after running the procedure 50 times for each of the settings. The horizontal dashed line defines the rejection threshold that has been computed using the data from the source: once the lower bound on the target risk (solid lines) exceeds this value, the null hypothesis is rejected. When clean MNIST data is passed to the network, drop in performance is not observed. Moreover, among the three shift types we observe both benign and harmful shifts. While to a human eye the translate effect is arguably the least harmful one, it is the most harmful to the performance of a network. This observation is also consistent with findings of Mu & Gilmer [13] who observe that if trained on a clean MNIST data without any data augmentation, CNNs tend to fail under the this effect. We refer the reader to Appendix E where we validate this observation by retraining the network several times.

Tracking the risk of a set-valued predictor on CIFAR-10-C dataset Here, using a ResNet-32 architecture as an underlying model, after training, we transform it into a set-valued predictor so that the miscoverage risk (equation 4) is controlled at level $\beta = 0.1$ with probability at least 0.95 [1]. That is achieved by keeping an extra held-out set, *calibration set*, used to tune the parameters of a wrapper built on top of the original model. We refer the reader to Appendix E for more details regarding this step. For each run, CIFAR-10 test set is split at random into three parts used for: (a) transforming a network into a set-valued

predictor (1000 points), (b) estimating an upper confidence bound on the miscoverage risk on the source (1000 points), and (c) evaluation purposes on either clean or corrupted images. We take $\varepsilon_{\text{tol}} = 0.05$, that is raising an alarm happens whenever coverage of the prediction sets on the target drops by 5%. Figure 6b illustrates that only the most severe version of the fog effect consistently leads to a significant increase in miscoverage. In Appendix E, we consider transforming the network into a set-valued predictor by taking $\beta = 0.05$, that is setting a lower prescribed error level. In particular, it results in larger prediction sets, which partially mitigates the effect of the fog on the drop in coverage.

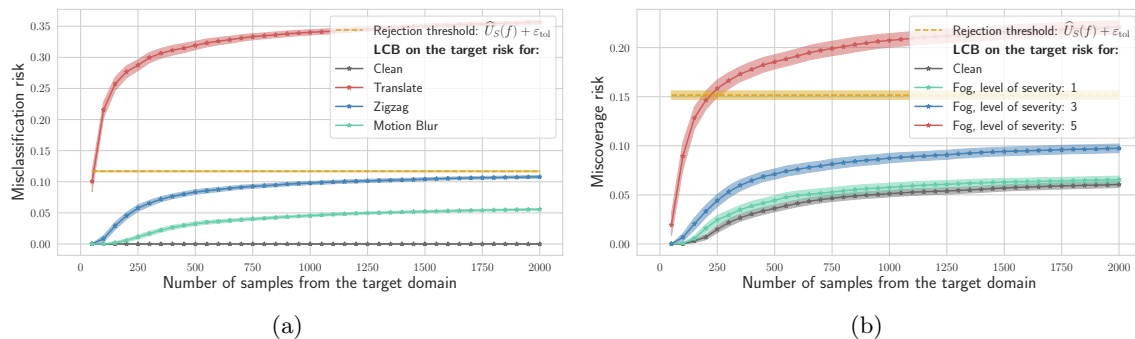


Figure 6: (a) Performance of the testing framework on MNIST-C dataset. Only the translation effect is consistently harmful to the classification performance of a CNN trained on clean data. (b) Performance of the testing framework on CIFAR-10-C dataset. Only the most severe version of the fog lead to a significant degradation in performance measured by a decrease in coverage of a set-valued predictor trained on top of a model trained on clean data.

4 Discussion

An important component of building reliable machine learning systems is enabling them to alarm a user when potentially unsafe behavior is observed, instead of allowing them to fail silently. In this work, we considered one particular failure scenario which deployed models constantly encounter in the real world — presence of distribution shifts. For differentiating benign and harmful settings, we developed a set of tools for testing in a data-adaptive way whether the performance of a model on the test data becomes significantly worse than the performance on the training data. The proposed framework is based on performing sequential estimation, and thus requires observing true labels for test data (possibly, in a delayed fashion). Across various types of distribution shifts considered in this work, it demonstrated promising empirical performance when distinguishing between harmful and benign ones.

Acknowledgements The authors thank Ian Waudby-Smith for fruitful discussions and giving feedback on an early version of this paper. The authors acknowledge support from NSF DMS 1916320 and an ARL IoBT CRA grant. Research reported in this paper was sponsored in part by the DEVCOM Army Research Laboratory under Cooperative Agreement W911NF-17-2-0196 (ARL IoBT CRA). The views and conclusions contained in this document are those of the authors and should not be interpreted as representing the official policies, either expressed or implied, of the Army Research Laboratory or the U.S. Government. The U.S. Government is authorized to reproduce and distribute reprints for Government purposes notwithstanding any copyright notation herein.

References

- [1] Stephen Bates, Anastasios Nikolas Angelopoulos, Lihua Lei, Jitendra Malik, and Michael I. Jordan. Distribution-free, risk-controlling prediction sets. *Journal of the ACM (to appear)*, 2021.

- [2] Glenn W. Brier. Verification of forecasts expressed in terms of probability. *Monthly Weather Review*, 78, 1950.
- [3] Yaroslav Ganin, Evgeniya Ustinova, Hana Ajakan, Pascal Germain, Hugo Larochelle, François Laviolette, Mario March, and Victor Lempitsky. Domain-adversarial training of neural networks. *Journal of Machine Learning Research*, 17(59):1–35, 2016.
- [4] Arthur Gretton, Karsten M. Borgwardt, Malte J. Rasch, Bernhard Schölkopf, and Alexander Smola. A kernel two-sample test. *Journal of Machine Learning Research*, 2012.
- [5] Chirag Gupta and Aaditya Ramdas. Top-label calibration and multiclass-to-binary reductions. *arXiv preprint: 2107.08353*, 2021.
- [6] Chirag Gupta, Aleksandr Podkopaev, and Aaditya Ramdas. Distribution-free binary classification: prediction sets, confidence intervals and calibration. In *Advances in Neural Information Processing Systems*, 2020.
- [7] Dan Hendrycks and Thomas Dietterich. Benchmarking neural network robustness to common corruptions and perturbations. In *International Conference on Learning Representations*, 2019.
- [8] Steven R. Howard, Aaditya Ramdas, Jon McAuliffe, and Jasjeet Sekhon. Time-uniform, nonparametric, nonasymptotic confidence sequences. *The Annals of Statistics*, 2021.
- [9] Xiaoyu Hu and Jing Lei. A distribution-free test of covariate shift using conformal prediction. *arXiv preprint: 2010.07147*, 2020.
- [10] Vathy M. Kamulete. Test for non-negligible adverse shifts. *arXiv preprint: 2107.02990*, 2021.
- [11] Alex Krizhevsky. Learning multiple layers of features from tiny images. Technical report, University of Toronto, 2009.
- [12] G. Lorden. Procedures for reacting to a change in distribution. *The Annals of Mathematical Statistics*, 42(6):1897 – 1908, 1971.
- [13] Norman Mu and Justin Gilmer. MNIST-C: A robustness benchmark for computer vision. *arXiv preprint arXiv:1906.02337*, 2019.
- [14] Aleksandr Podkopaev and Aaditya Ramdas. Distribution free uncertainty quantification for classification under label shift. *Conference on Uncertainty in Artificial Intelligence*, 2021.
- [15] Joaquin Quionero-Candela, Masashi Sugiyama, Anton Schwaighofer, and Neil D. Lawrence. *Dataset Shift in Machine Learning*. The MIT Press, 2009.
- [16] Stephan Rabanser, Stephan Günnemann, and Zachary Lipton. Failing loudly: An empirical study of methods for detecting dataset shift. In *Advances in Neural Information Processing Systems*, 2019.
- [17] Marco Saerens, Patrice Latinne, and Christine Decaestecker. Adjusting the outputs of a classifier to new a priori probabilities: A simple procedure. *Neural Computation*, 2002.
- [18] Hidetoshi Shimodaira. Improving predictive inference under covariate shift by weighting the log-likelihood function. *Journal of Statistical Planning and Inference*, 2000.
- [19] Ryan J Tibshirani, Rina Foygel Barber, Emmanuel Candes, and Aaditya Ramdas. Conformal prediction under covariate shift. In *Advances in Neural Information Processing Systems*, 2019.
- [20] Vladimir Vovk. Testing for concept shift online. *arXiv preprint: 2012.14246*, 2020.
- [21] Vladimir Vovk. Testing randomness online. *Statistical Science (to appear)*, 2020.
- [22] Vladimir Vovk, Alex Gammerman, and Glenn Shafer. *Algorithmic learning in a random world*. Springer, 2005.

- [23] Vladimir Vovk, Ivan Petej, Ilya Nouretdinov, Ernst Ahlberg, Lars Carlsson, and Alex Gammerman. Retrain or not retrain: conformal test martingales for change-point detection. In *Proceedings of the Tenth Symposium on Conformal and Probabilistic Prediction and Applications*, 2021.
- [24] Abraham Wald. Sequential tests of statistical hypotheses. *The Annals of Mathematical Statistics*, 16(2):117 – 186, 1945.
- [25] Ian Waudby-Smith and Aaditya Ramdas. Estimating means of bounded random variables by betting. *arXiv preprint: 2010:09686*, 2021.
- [26] Yifan Wu, Ezra Winston, Divyansh Kaushik, and Zachary Lipton. Domain adaptation with asymmetrically-relaxed distribution alignment. In *International Conference on Machine Learning*, 2019.

A Brier score in the multiclass setting

This section contains derivations of decompositions stated in Section 2 and comparisons between introduced versions of the Brier score.

Brier score decompositions The expected Brier score for the case when the whole output vector is considered satisfies the following decomposition:

$$\begin{aligned}
 2 \cdot R^{\text{brier}}(f) &= \mathbb{E} \|f(X) - h(Y)\|^2 \\
 &= \mathbb{E} \|f(X) - c(X) + c(X) - h(Y)\|^2 \\
 &\stackrel{(a)}{=} \mathbb{E} \|f(X) - c(X)\|^2 + \mathbb{E} \|c(X) - h(Y)\|^2 \\
 &= \mathbb{E} \|f(X) - c(X)\|^2 + \mathbb{E} \|c(X) - \mathbb{E}[c(X)] + \mathbb{E}[c(X)] - h(Y)\|^2 \\
 &\stackrel{(b)}{=} \underbrace{\mathbb{E} \|f(X) - c(X)\|^2}_{\text{calibration error}} - \underbrace{\mathbb{E} \|c(X) - \mathbb{E}[c(X)]\|^2}_{\text{sharpness}} + \underbrace{\mathbb{E} \|h(Y) - \mathbb{E}[h(Y)]\|^2}_{\text{intrinsic uncertainty}}.
 \end{aligned}$$

Above, (a) follows by conditioning on $f(X)$ for the cross-term and recalling that $\mathbb{E}[h(Y) | f(X)] = c(X)$, (b) also follows by conditioning on $f(X)$ and noticing that $\mathbb{E}[h(Y)] = \mathbb{E}[c(X)]$. Now, recall that a predictor is (canonically) calibrated if $f(X) \stackrel{a.s.}{=} c(X)$, in which case the calibration error term is simply zero. Next, we consider the top-label Brier score $\ell^{\text{brier-top}}$. Following essentially the same argument as before, we get that:

$$\begin{aligned}
 &\mathbb{E} [\ell^{\text{brier-top}}(f(X), Y)] \\
 &= \mathbb{E} (f_{\hat{y}(X;f)}(X) - h_{\hat{y}(X;f)}(Y))^2 \\
 &= \mathbb{E} (f_{\hat{y}(X;f)}(X) - c^{\text{top}}(X) + c^{\text{top}}(X) - h_{\hat{y}(X;f)}(Y))^2 \\
 &= \mathbb{E} (f_{\hat{y}(X;f)}(X) - c^{\text{top}}(X))^2 + \mathbb{E} (c^{\text{top}}(X) - h_{\hat{y}(X;f)}(Y))^2 \\
 &= \underbrace{\mathbb{E} (f_{\hat{y}(X;f)}(X) - c^{\text{top}}(X))^2}_{\text{top-label calibration error}} - \underbrace{\mathbb{E} (c^{\text{top}}(X) - \mathbb{E}[c^{\text{top}}(X)])^2}_{\text{top-label sharpness}} + \underbrace{\text{Var}(h_{\hat{y}(X;f)}(Y))}_{\text{variance of the misclassification loss}}.
 \end{aligned}$$

Note that in contrast to the classic Brier score decomposition, the last term in this decomposition depends only on the top-class prediction of the underlying predictor, and thus on its accuracy.

Comparison of the scores in multiclass setting Recall that the difference between three versions of the Brier score arises when one moves beyond the binary classification setting. We illustrate the difference by considering a 4-class classification problem where the data represent a balanced (that is all classes are equally likely) mixture of 4 Gaussians with identity covariance matrix and mean vectors being the vertices of a 2-dimensional unit cube. One such sample is presented on Figure 7a.

Next, we analyze locally the Brier scores when the Bayes-optimal rule is used as an underlying predictor, that is we split the area into small rectangles and estimate the mean score within each rectangle by a sample average. The results are presented on Figures 7b, 7c and 7d. Note that the difference between the assigned scores is mostly observed for the points that lie at the intersection of 4 classes where the support of the corresponding output vectors is large.

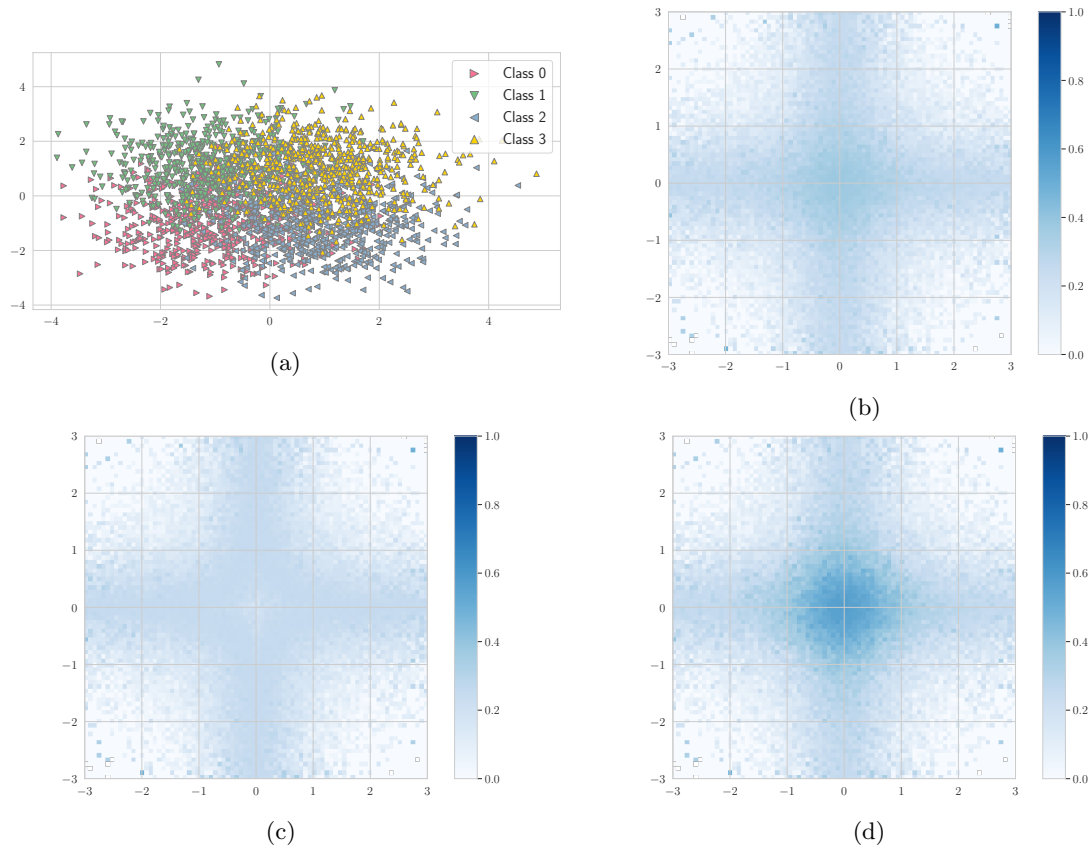


Figure 7: (a) Visualization of 4-class classification problem with all classes being equally likely; (b) localized classic Brier score ℓ^{brier} (equation 1); (c) localized top-label Brier score $\ell^{\text{brier-top}}$ (equation 2); (d) localized true-class Brier score $\ell^{\text{brier-true}}$ (equation 3).

Brier scores under label shift Here we consider the case when label shift on the target domain is present. First, introduce the label likelihood ratios, also known as the importance weights, $w_y := \pi_y^T / \pi_y^S$, $y \in \mathcal{Y}$. For measuring the strength of the shift, we introduce the *condition number*: $\kappa = \sup_y w_y / \inf_{y:w_y \neq 0} w_y$. Note that when the shift is not present, the condition number $\kappa = 1$. To evaluate the sensitivity of the losses to the presence of label shift, we proceed as follows: first, the class proportions for both source and target domains are sampled from the Dirichlet distribution (to avoid extreme class proportion, we perform truncation at levels 0.15 and 0.85 and subsequent renormalization). Then we use the Bayes-optimal rule for the source domain to perform predictions on the target and compute the corresponding losses. On Figure 8, we illustrate relative increase in the average Brier scores plotted against the corresponding condition number when all data points are considered (Figure 8a) and when attention is restricted to the area where classes highly intersect (Figure 8b). In general, all three versions of the Brier score suffer similarly on average, but in the localized area where classes highly intersect, the top-label Brier score does not increase significantly under label shift.

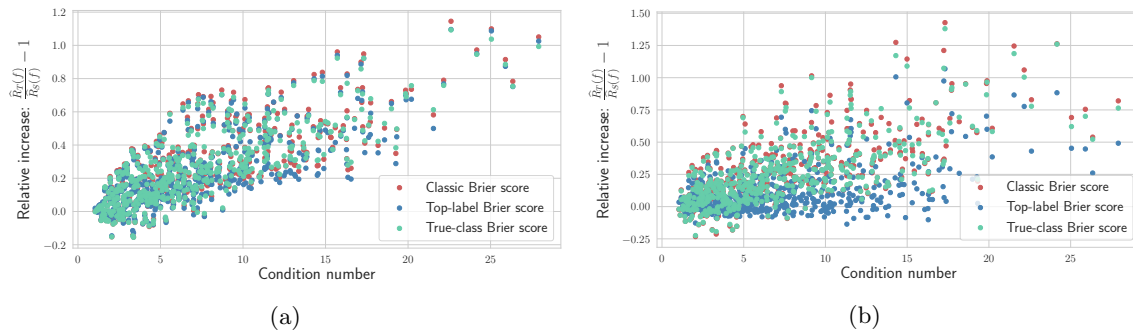


Figure 8: (a) Relative increase for different versions of the Brier score in the multiclass setting under label shift; (b) Relative increase for different versions of the Brier score in the multiclass setting under label shift when attention is restricted to the area where classes highly intersect (cube with vertices at $(\pm 1/2, \pm 1/2)$). While in general, all three versions of the Brier score suffer similarly on average, in the localized area where classes highly intersect, the top-label Brier score does not increase significantly under label shift.

B Proofs

Proof of Proposition 1. For brevity, we omit writing f for the source/target risks and the corresponding bound upper/lower confidence bounds. Starting with the absolute change and the null $H_0 : R_T - R_S \leq \varepsilon_{\text{tol}}$, we have:

$$\begin{aligned} & \mathbb{P}_{H_0} \left(\exists t \geq 1 : \widehat{L}_T^{(t)} > \widehat{U}_S + \varepsilon_{\text{tol}} \right) \\ &= \mathbb{P}_{H_0} \left(\exists t \geq 1 : \left(\widehat{L}_T^{(t)} - R_T \right) - \left(\widehat{U}_S - R_S \right) > \varepsilon_{\text{tol}} - (R_T - R_S) \right) \\ &\leq \mathbb{P}_{H_0} \left(\exists t \geq 1 : \left(\widehat{L}_T^{(t)} - R_T \right) - \left(\widehat{U}_S - R_S \right) > 0 \right). \end{aligned}$$

Note that $\exists t \geq 1 : \left(\widehat{L}_T^{(t)} - R_T \right) - \left(\widehat{U}_S - R_S \right) > 0$ implies that either $\exists t \geq 1 : \widehat{L}_T^{(t)} - R_T > 0$ or $\widehat{U}_S - R_S < 0$. Thus, invoking union bound yields:

$$\begin{aligned} & \mathbb{P}_{H_0} \left(\exists t \geq 1 : \left(\widehat{L}_T^{(t)} - R_T \right) - \left(\widehat{U}_S - R_S \right) > 0 \right) \\ &\leq \mathbb{P} \left(\exists t \geq 1 : \widehat{L}_T^{(t)} - R_T > 0 \right) + \mathbb{P} \left(\widehat{U}_S - R_S < 0 \right) \\ &\leq \delta_T + \delta_S, \end{aligned}$$

by construction and validity guarantees for $\widehat{L}_T^{(t)}$ and \widehat{U}_S . Similarly, considering the relative change, i.e., the null: $H'_0 : R_T \leq (1 + \varepsilon'_{\text{tol}})R_S$, we have:

$$\begin{aligned} & \mathbb{P}_{H'_0} \left(\exists t \geq 1 : \widehat{L}_T^{(t)} > (1 + \varepsilon'_{\text{tol}})\widehat{U}_S \right) \\ &= \mathbb{P}_{H'_0} \left(\exists t \geq 1 : \left(\widehat{L}_T^{(t)} - R_T \right) - (1 + \varepsilon'_{\text{tol}}) \left(\widehat{U}_S - R_S \right) > (1 + \varepsilon'_{\text{tol}})R_S - R_T \right) \\ &\leq \mathbb{P}_{H'_0} \left(\exists t \geq 1 : \left(\widehat{L}_T^{(t)} - R_T \right) - (1 + \varepsilon'_{\text{tol}}) \left(\widehat{U}_S - R_S \right) > 0 \right). \end{aligned}$$

Similarly, note that $\exists t \geq 1 : \left(\widehat{L}_T^{(t)} - R_T \right) - (1 + \varepsilon'_{\text{tol}}) \left(\widehat{U}_S - R_S \right) > 0$ implies that either $\exists t \geq 1 : \widehat{L}_T^{(t)} - R_T > 0$ or $\widehat{U}_S - R_S < 0$. Thus, invoking union bound yields the desired result. \square

C Primer on the upper and lower confidence bounds

This section contains the details for the concentration results used in this work. Results presented in this section are not new were developed in a series of recent works [8, 25]. We follow the notation from Waudby-Smith & Ramdas [25] for consistency and use the superscript (t) when referring to confidence sequences (CS) and (n) when referring to confidence intervals (CI).

Hoeffding's confidence intervals / sequences Then the upper and lower endpoints of the predictably-mixed Hoeffding's CS are given by:

$$\begin{aligned} L_{\text{PM-H}}^{(t)} &:= \left(\frac{\sum_{i=1}^t \lambda_i Z_i}{\sum_{i=1}^t \lambda_i} - \frac{\log(1/\delta) + \sum_{i=1}^t \psi_H(\lambda_i)}{\sum_{i=1}^t \lambda_i} \right), \\ U_{\text{PM-H}}^{(t)} &:= \left(\frac{\sum_{i=1}^t \lambda_i Z_i}{\sum_{i=1}^t \lambda_i} + \frac{\log(1/\delta) + \sum_{i=1}^t \psi_H(\lambda_i)}{\sum_{i=1}^t \lambda_i} \right), \end{aligned}$$

where $\psi_H(\lambda) := \lambda^2/8$ and $\lambda_1, \lambda_2, \dots$ is a predictable mixture. We use a particular predictable mixture given by:

$$\lambda_t^{\text{PM-H}} := \sqrt{\frac{8 \log(1/\delta)}{t \log(t+1)}} \wedge 1.$$

When approximating the risk on the source domain, one would typically have a held-out sample of a fixed size n , and so one could either use the classic upper limit of the Hoeffding's confidence interval, which is recovered by taking equal $\lambda_i = \lambda = \sqrt{8 \log(1/\delta)/n}$, $i = 1, \dots, n$, in which case the upper and lower limits simplify to:

$$L_H^{(n)} := \left(\frac{\sum_{i=1}^n Z_i}{n} - \sqrt{\frac{\log(1/\delta)}{2n}} \right), \quad U_H^{(n)} := \left(\frac{\sum_{i=1}^n Z_i}{n} + \sqrt{\frac{\log(1/\delta)}{2n}} \right),$$

or by considering running intersection of the predictably mixed Hoeffding's confidence sequence: $(\min_{t \leq n} U_{\text{PM-H}}^{(t)}, \max_{t \leq n} L_{\text{PM-H}}^{(t)})$.

Empirical-Bernstein confidence intervals / sequences The upper and lower endpoints of the predictably-mixed empirical Bernstein confidence sequences are given by:

$$L_{\text{PM-EB}}^{(t)} := \frac{\sum_{i=1}^t \lambda_i Z_i}{\sum_{i=1}^t \lambda_i} - \frac{\log(1/\delta) + \sum_{i=1}^t v_i \psi_E(\lambda_i)}{\sum_{i=1}^t \lambda_i},$$

$$U_{\text{PM-EB}}^{(t)} := \frac{\sum_{i=1}^t \lambda_i Z_i}{\sum_{i=1}^t \lambda_i} + \frac{\log(1/\delta) + \sum_{i=1}^t v_i \psi_E(\lambda_i)}{\sum_{i=1}^t \lambda_i},$$

where

$$v_i := 4(X_i - \hat{\mu}_{i-1})^2, \quad \text{and} \quad \psi_E(\lambda) := (-\log(1-\lambda) - \lambda)/4, \quad \text{for } \lambda \in [0, 1].$$

One particular choice of a predictable mixture $(\lambda_t^{\text{PM-EB}})_{t=1}^\infty$ is given by:

$$\lambda_t^{\text{PM-EB}} := \sqrt{\frac{2 \log(1/\delta)}{\hat{\sigma}_{t-1}^2 t \log(1+t)}} \wedge c, \quad \hat{\sigma}_t^2 := \frac{\frac{1}{4} + \sum_{i=1}^t (Z_i - \hat{\mu}_i)^2}{t+1}, \quad \hat{\mu}_t := \frac{\frac{1}{2} + \sum_{i=1}^t Z_i}{t+1},$$

for some $c \in (0, 1)$. We use $c = 1/2$ and also set $\hat{\mu}_0 = 1/2$, $\hat{\sigma}_0 = 1/4$. If given a sample of a fixed size n , we consider running intersection along with the predictable sequence given by:

$$\lambda_t^{\text{PM-EB}} = \sqrt{\frac{2 \log(1/\delta)}{n \hat{\sigma}_{t-1}^2}} \wedge c, \quad t = 1, \dots, n.$$

Betting-based confidence intervals / sequences Tighter confidence intervals/sequences can be obtained by invoking tools from martingale analysis and deploying betting strategies for confidence intervals/sequences construction proposed in [25]. While those can not be computed in closed-form, empirically they tend to outperform previously considered confidence intervals/sequences. Recall that we are primarily interested in one-sided results, and for simplicity we discuss. For any $m \in [0, 1]$, introduce a capital (wealth) process:

$$\mathcal{K}_t^\pm(m) := \prod_{i=1}^t (1 \pm \lambda_i^\pm(m) \cdot (X_i - m)),$$

where $\{\lambda_t^+(m)\}_{t=1}^\infty$ and $\{\lambda_t^-(m)\}_{t=1}^\infty$ are $[0, 1/m]$ -valued and $[0, 1/(1-m)]$ -valued predictable sequences respectively. A particular example of such predictable sequences we use is given by:

$$\lambda_t^+(m) := \left| \dot{\lambda}_t^+ \right| \wedge \frac{c}{m}, \quad \lambda_t^-(m) := \left| \dot{\lambda}_t^- \right| \wedge \frac{c}{1-m},$$

where, for example, $c = 1/2$ or $3/4$ and $\dot{\lambda}_t^\pm$ do not depend on m . Such choice guarantees, in particular, that the resulting martingale is nonnegative. For example, the wealth process $\mathcal{K}_t^+(m)$ incorporates a belief that the true mean μ is larger than m and the converse belief is incorporated in $\mathcal{K}_t^-(m)$, that is, the wealth is expected to be accumulated under the corresponding belief (e.g., consider $m = 0$ and the corresponding $\mathcal{K}_t^+(0)$ with a high value, and $m = 1$ and the corresponding $\mathcal{K}_t^+(1)$ with a low value). Using that $\mathcal{K}_t^+(m)$ is

non-increasing in m , i.e., $m_2 \geq m_1$, then $\mathcal{K}_t^+(m_2) \leq \mathcal{K}_t^+(m_1)$, we thus can use grid search (up to specified approximation error Δ_{grid}) to efficiently approximate $L_{\text{Bet}}^{(t)} = \inf B_t^+$, where

$$\mathcal{B}_t^+ := \{m \in [0, 1] : \mathcal{K}_t^+(m) < 1/\delta\},$$

that is, the collection of all m for which that the capital wasn't accumulated. Then we can consider $L_{\text{Bet}}^{(n)} = \max_{t \leq n} L_{\text{Bet}}^{(t)}$. When $m = \mu$ is considered, none of $\mathcal{K}_t^\pm(\mu)$ is expected to be large, since by Ville's inequality:

$$\mathbb{P}(\exists t \geq 1 : \mathcal{K}_t^+(\mu) \geq 1/\delta) \leq \delta,$$

and thus we know that with high probability the true mean is larger than $L_{\text{Bet}}^{(n)}$. That is,

$$\begin{aligned} \mathbb{P}(\mu < L_{\text{Bet}}^{(n)}) &= \mathbb{P}\left(\mu < \max_{t \leq n} L_{\text{Bet}}^{(t)}\right) = \mathbb{P}(\exists t \geq 1 : \mu < \inf B_t^+) \\ &= \mathbb{P}(\exists t \geq 1 : \mathcal{K}_t^+(\mu) \geq 1/\delta) \leq \delta. \end{aligned}$$

By a similar argument, we get that with high probability, the true mean is less than $U_{\text{Bet}}^{(n)} = \min_{t \leq n} \sup B_t^-$:

$$\begin{aligned} \mathbb{P}(\mu > U_{\text{Bet}}^{(n)}) &= \mathbb{P}\left(\mu > \min_{t \leq n} \sup B_t^-\right) = \mathbb{P}(\exists t \geq 1 : \mu > \sup B_t^-) \\ &= \mathbb{P}(\exists t \geq 1 : \mathcal{K}_t^-(\mu) \geq 1/\delta) \leq \delta. \end{aligned}$$

D Experiments on simulated data

Figure 9 illustrates data samples for two settings where the presence of label shift is not expected to cause degradation in model performance (measured in terms of absolute increase in misclassification risk) for the first one ($\mu_0 = (-2, 0)^\top$, $\mu_1 = (2, 0)^\top$), but label shift may potentially degrade performance for the second ($\mu_0 = (-1, 0)^\top$, $\mu_1 = (1, 0)^\top$). For both cases, samples follow the same data generation pipeline as in Section 1 with only changes in class centers.

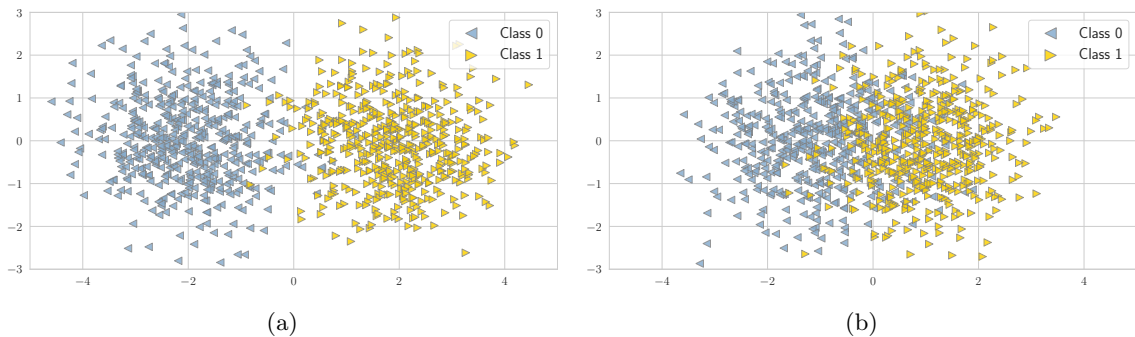


Figure 9: (a) Simulated dataset with well-separated classes. Presence of label shift presumably will not lead to a high absolute increase in the misclassification risk. (b) In contrast, when the classes are *not* well-separated, presence of label shift presumably might hurt the misclassification risk.

D.1 Brier score as a target metric

Here we replicate the empirical study from Section 3.1 but use the Brier score as a target metric. Recall that all three multiclass versions of the Brier score discussed in this work reduce to the same loss in the binary setting. First, we compare upper confidence bounds for the Brier score computed by invoking different concentration results on Figure 10. Similar to the misclassification risk, variance-adaptive confidence bounds exploit the low-variance structure and are tighter when compared against the non-adaptive one.

Next, we perform empirical analysis of the power of the testing framework. We take $\varepsilon_{\text{tol}} = 0.1$ which corresponds to testing for a 10% relative increase in the Brier score. We take $n_S = 1000$ data points from the source distribution to compute the upper confidence bound on the source risk $\widehat{U}_S(f)$. Subsequently, we sample the data from the target distribution in batches of 50, with maximum number of samples from the target set to be 2000. On Figure 10b, we present the proportion of cases when the null hypothesis is rejected out of 250 simulations performed for each candidate class 1 probability. On Figure 10c, we illustrate average sample size from the target domain that was needed to reject the null hypothesis. When a stronger and more harmful label shift is present, less samples are required to reject the null, and moreover, the most powerful tests utilize upper/lower confidence bounds obtained via the betting approach. On Figure 10d, we present the comparison of different time-uniform lower confidence bounds.

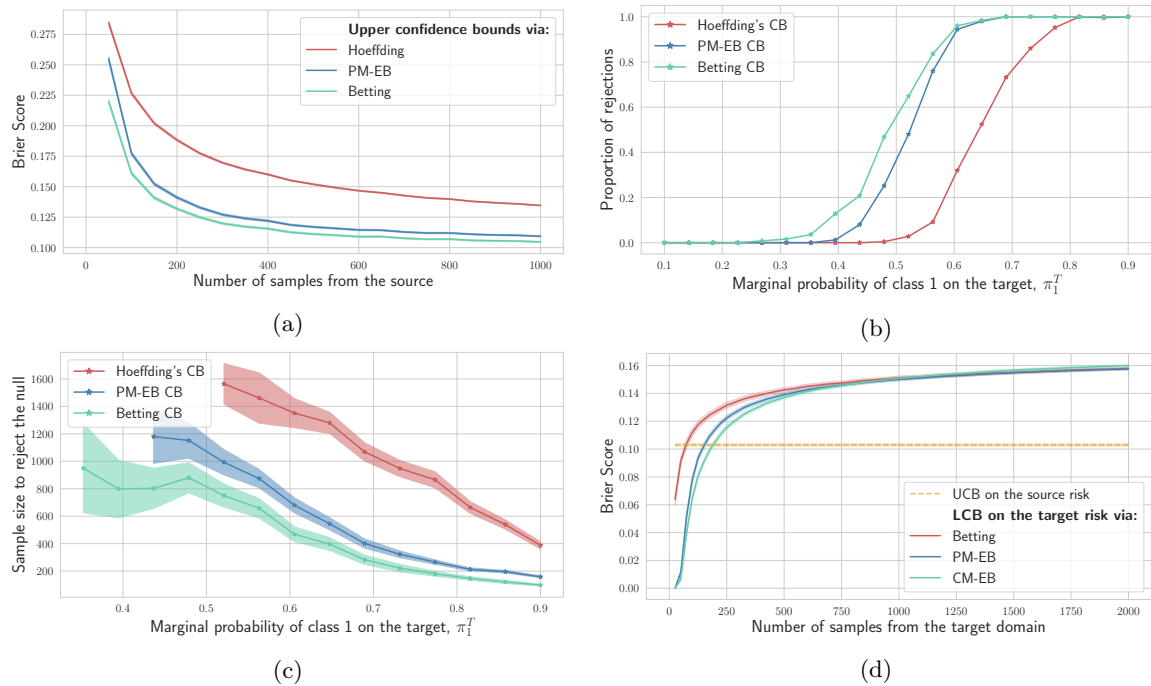


Figure 10: (a) Upper confidence bounds $\widehat{U}_S(f)$ on the Brier score for the source domain. Similar to the misclassification risk, variance-adaptive confidence bounds are tighter when compared against the Hoeffding's one. For each fixed number of data points from the source domain used to compute $\widehat{U}_S(f)$, presented results are aggregated over 1000 random data draws. (b) Proportion of null rejections made by the procedure when testing for 10% relative increase of the Brier score. (c) Average sample size from the target distribution that was needed to reject the null. Invoking tighter concentration results allows to raise an alarm after processing less samples from the target domain. (d) Different lower/upper confidence bounds on the target/source domain for the Brier score.

E Experiments on real datasets

E.1 MNIST-C simulation

Architecture and training For MNIST-C dataset, we train a shallow CNN with two convolutional layers (each with 3×3 kernel matrices), each followed by max-pooling layers. Subsequently, the result is flattened and followed by a dropout layer ($p = 0.5$), a fully-connected layer with 128 neurons and an output layer. Note that the network is trained on original (clean) MNIST data, which is split split into two folds with 10% of data used for validation purposes. All images are scaled to $[0, 1]$ range before the training is performed.

Training multiple networks To validate observations regarding shift malignancy from Section 3.2, we train 5 different networks (following the same training protocol) and report aggregated (over 25 random ordering of the data from the target) results on Figure 11. The observation that applying translation to the MNIST images represents a harmful shift is consistent across all networks.

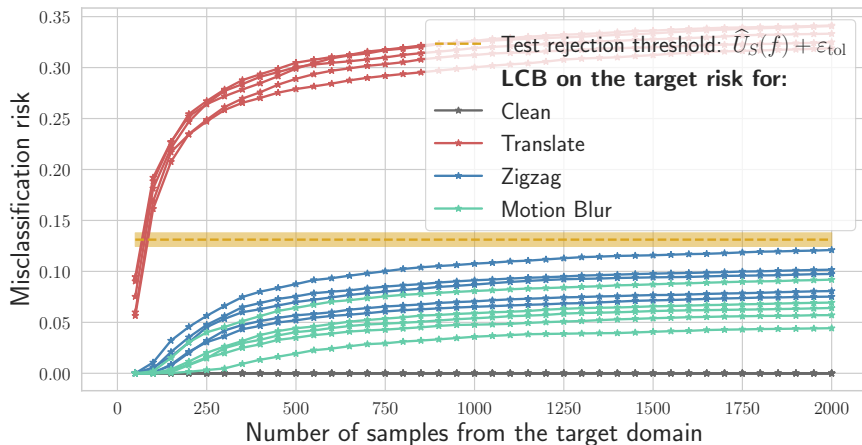


Figure 11: Lines of the same color correspond to 5 different CNNs. For each network, the results aggregated over 25 random runs of the testing framework for randomly permuted test data. Applying translate effect is consistently harmful to the performance of CNNs trained on clean MNIST data. The bar around the yellow dashed line corresponds to 2 standard deviations.

E.2 CIFAR-10-C simulation

Architecture and training The model underlying a set-valued predictor is a standard ResNet-32. It is trained for 50 epochs on the original (clean) CIFAR-10 dataset, without data augmentation, using 10% of data for validation purposes. All images are scaled to $[0, 1]$ range before the training is performed. The accuracy of the resulting network is $\approx 80.5\%$.

Transforming a point predictor into a set-valued one To transform a point predictor into a set-valued one, we consider a sequence of candidate prediction sets $S_\lambda(x)$, parameterized by univariate parameter λ , with larger λ leading to larger prediction sets. Under the considered setting, the underlying predictor is an estimator of the true conditional probabilities $\pi_y(x) = \mathbb{P}(Y = y | X = x)$. Given a learnt predictor f , we can define

$$\rho_y(x; f) := \sum_{k=1}^K f_k(x) \cdot \mathbb{1}\{f_k(x) > f_y(x)\}$$

to represent estimated probability mass of the labels that are more likely than y . Subsequently, we can consider the following sequence of set-valued predictors:

$$S_\lambda(x) = \{y \in \mathcal{Y} : \rho_y(x; f) \leq \lambda\}, \quad \lambda \in \Lambda := [0, 1],$$

that is the sequence is based on the estimated density level sets, starting by including the most likely labels according to the predictions of f . To tune the parameter λ , we follow Bates et al. [1]: we keep a labeled held-out *calibration set*, and use it to pick:

$$\hat{\lambda} = \inf \left\{ \lambda \in \Lambda : \hat{R}^+(\lambda') < \beta, \forall \lambda' > \lambda \right\},$$

where $\hat{R}^+(\lambda')$ is an upper confidence bound for the risk function at level β . The resulting set-valued predictor is then (β, γ) -RCPS, that is,

$$\mathbb{P}(R(S_{\hat{\lambda}}) \leq \beta) \geq 1 - \gamma,$$

under the i.i.d. assumption. More details and validity guarantees can be found in Bates et al. [1].

Set-valued predictor for $\beta = 0.05$ used as a prescribed error level of a set-valued predictor We also consider decreasing β parameter to 0.05, which in words, corresponds to increasing a desired coverage level. Figure 12a compares average sizes of the prediction sets for two candidate values: $\beta_1 = 0.05$ and $\beta_2 = 0.1$, when the set-valued predictor is passes either clean CIFAR-10 data, or images to which fog corruption has been applied. As expected, decreasing β leads to larger prediction sets on average, with the size increasing when corrupted images are passes as input, that the size reflects uncertainty in prediction. In Figure 12b, we observe that when we run the testing framework for the set-valued predictor corresponding to $\beta = 0.05$, only the most severe version of corruptions by adding fog is consistently marked as harmful, and thus raising an alarm. Similar to Section 3.2, we also use $\varepsilon_{\text{tol}} = 0.05$.

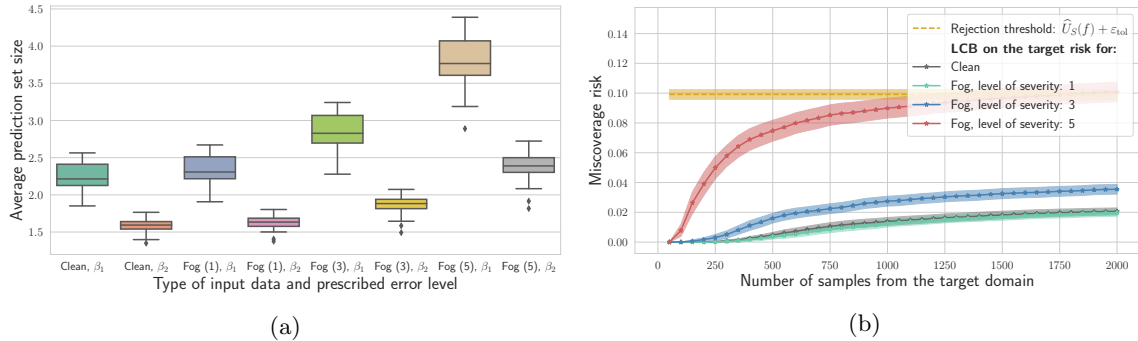


Figure 12: (a) Average size of prediction sets for $\beta_1 = 0.05$ and $\beta_2 = 0.1$ and different types of input data. First, lower beta, corresponding to higher desired coverage, leads to larger prediction sets on average. Second, average size of the prediction sets increases when more corrupted images are passed as input, thus reflecting uncertainty in prediction. (b) Results of running the framework when $\beta_1 = 0.05$ is used to construct a wrapper. Observe that setting a lower prescribed error level β and thus enlarging resulting prediction sets partially mitigates the impact of corrupting images with the fog effect. However, the most severe form of such corruption still consistently leads to rejecting the null. The bars around dashed and solid lines correspond to 2 standard deviations.